Primary saturation of α,β-unsaturated carbonyl containing fatty acids does not abolish electrophilicity

Nathaniel W. Snyder [‡, &], Bhupinder Singh[*, &], Gregory Buchan[*], James O'Brien[*], Alejandro D. Arroyo[^], Xiaojing Liu[†], Robert W. Sobol[*, #], Ian A. Blair[^], Clementina A. Mesaros[^], and Stacy Gelhaus Wendell [*]

[‡] Center for Metabolic Disease Research, Department of Microbiology and Immunology, Lewis Katz School of Medicine, Temple University, Philadelphia, PA, 19140, USA

* Department of Pharmacology and Chemical Biology, University of Pittsburgh, Pittsburgh, PA, 15261

[^]Centers for Cancer Pharmacology and Excellence in Environmental Toxicology, Department of Pharmacology, University of Pennsylvania, Philadelphia, PA, 19104

[†] Department of Molecular and Structural Biology, NC State, Raleigh, NC 27695

[#]University of South Alabama, Mitchell Cancer Institute, Mobile, AL, 36688

[&]These authors contributed equally to this work

Co-Corresponding authors:

Stacy Gelhaus Wendell

Department of Pharmacology & Chemical Biology, University of Pittsburgh

200 Lothrop Street, BST E1340, Pittsburgh, PA 15261

Email: gstacy@pitt.edu

Phone: 412-648-9319

Fax: 412-648-2229

Nathaniel W. Snyder

Center for Metabolic Disease Research, Department of Microbiology and Immunology,

Lewis Katz School of Medicine at Temple University,

Philadelphia, PA, 19140, USA

Email: NateWSnyder@temple.edu

Running Title: Unconventional saturation of oxo fatty acids

Abbreviations: 15-deoxy-$\Delta^{12,14}$-PGJ_2 (15d-PGJ_2); 15-prostaglandin dehydrogenase (15-PGDH); arachidonic acid (AA); β-mercaptoethanol (BME); Cyclooxygenase (COX);; hydroperoxyeicosatetraenoic acid (HPETE); human umbilical vein endothelial cells (HUVECs); lipoxygenase (LO); methyl ester (ME); oxoeicosatetraenoic acid (oxoETE); prostaglandin E_2 (PGE_2); prostaglandin E receptor (EP); prostaglandin reductase 1 (PTGR1), solid phase extraction (SPE)

Abstract

Metabolism of PUFA results in the formation of hydroxylated fatty acids that can be further oxidized by dehydrogenases, often resulting in the formation of electrophilic, α,β-unsaturated ketone containing fatty acids. As electrophiles are associated with redox signaling, we sought to investigate the metabolism of the oxo-fatty acid products in relation to their double bond architecture. Using an untargeted liquid chromatography mass spectrometry approach, we identified mono- and di-saturated products of the arachidonic acid-derived 11-oxoeicosatetraenoic acid (11-oxoETEs) and mono-saturated metabolites of 15-oxoETE and 17-oxoDHA in both human A549 lung carcinoma and umbilical vein endothelial cells. Notably, mono-saturated oxo-fatty acids maintained their electrophilicity as determined by nucleophilic conjugation to glutathione while a second saturation of 11-oxoETE resulted in a loss of electrophilicity. These results would suggest that prostaglandin reductase, known for its reduction of the α,β-unsaturated double bond, was not responsible for saturation of oxo-fatty acids. Surprisingly, the knock down of prostaglandin reductase by shRNA confirmed its participation in the formation of 15-oxoETE and 17-oxoDHA mono-saturated metabolites. These findings will further facilitate the study of electrophilic fatty acid metabolism and signaling in the context of inflammatory diseases and cancer where they have been shown to have anti-inflammatory and anti-proliferative signaling properties.

Key words: eicosanoids, dehydrogenase, fatty acid/metabolism, fatty acid/oxidation, mass spectrometry, oxoETE, KETE, prostaglandin reductase

Introduction

Omega-6 (Ω-6) and omega-3 (Ω-3) fatty acids are enzymatically metabolized by cyclooxygenases (COX), lipoxygenases (LO), and cytochrome P450s to numerous fatty acid metabolites, many of which are biologically active (1-4). Metabolism produces a diversity of structural alterations, some subtle, which result in a plethora of signaling actions. Initial hydrogen abstraction and oxygenation of parent fatty acids, such as arachidonic acid (AA, Ω-6) and docosahexaenoic acid (DHA, Ω-3) forms hydroperoxy fatty acids that are quickly reduced by peroxidases to their corresponding hydroxy metabolites, the AA-derived hydroxyeicosatetraenoic acids (HETEs) and the DHA-derived hydroxydocosahexaenoic acids (HDoHEs) (3, 5, 6). One predominant pathway of hydroxy fatty acid metabolism is oxidation by dehydrogenases, such as 15-hydroxyprostaglandin dehydrogenase (15PGDH), to their corresponding ketone-containing oxo-fatty acid products (7-9). These products contain an α,β-unsaturated carbonyl that presents electrophilic properties. Unlike many bioactive fatty acids, the electrophilic oxo-fatty acids, with the exception of 5- oxoeicosatetraenoic acid (oxoETE), are generally not known to signal through G-protein coupled receptors (GPCR), but form covalent Michael addition adducts with nucleophilic amino acids, such as cysteine, that are found in critical redox transcriptional regulatory proteins and pro-inflammatory enzymes (6, 10-12). Electrophilic α,β-unsaturated ketone containing fatty acids derived from Ω-6 and Ω-3 polyunsaturated fatty acids have anti-proliferative, anti-inflammatory, and redox signaling properties (13-16). While a great deal of focus has been placed on the

formation of electrophilic protein adduction and signaling (17, 18); very little is known about the downstream metabolism of these electrophilic fatty acids.

Based on the exemplary metabolism of 15-ketoprostaglandin E_2 (15-ketoPGE$_2$) to 13, 14-dihydro-15-ketoPGE$_2$, it is reasonable to hypothesize that other α,β-unsaturated carbonyl-containing electrophiles would follow a similar pathway of metabolism. 15-ketoPGE$_2$ is formed from the conversion of AA to PGH$_2$ by cyclooxygenase (COX) followed by prostaglandin E synthase formation of PGE$_2$. PGE$_2$ contains a hydroxyl group at C15 that is oxidized by 15PGDH to form 15-ketoPGE$_2$, an electrophile with bioactive signaling capabilities (19). Inactivation of the electrophilic moiety occurs via reduction of the α,β-unsaturated bond by prostaglandin reductase (PTGR)1, which is also commonly referred to as leukotriene B_4 12-hydroxydehydrogenase, 2-alkenal reductase, or alkenal/one oxidoreductase in humans and dithiolethione inducible gene in rat (7). Electrophile formation and subsequent reduction by PTGR1 is also documented for the AA-derived Lipoxin A_4 as well other prostaglandins and alkenals including 4-hydroxynonenal (20, 21). Recently, it was demonstrated that PTGR1 also reduces the double bond of the electrophile nitro-oleic acid, resulting in the non-electrophilic nitro-alkane, nitro-stearic acid (22).

Based on these data, one would assume that other α,β-unsaturated carbonyl-containing electrophiles, such as the oxoETEs and the oxodocosahexaenoic acids (oxoDHAs) would also be inactivated by PTGR1. In this current study, the metabolic fate of two oxoETEs derived from arachidonic acid, 11- and 15-oxoETE and the DHA-derived 17-oxoDHA, was investigated. Contrary to our original hypothesis, we show that the mono-saturated metabolite of all three oxo-fatty acids retains electrophilicity.

Materials and Methods

Reagents and materials. 11-oxoETE, 15-oxoETE, 11-oxoETE-methyl ester (11-oxoETE-ME), 15-oxoETE-methyl ester (15-oxoETE-ME) and the [$^{13}C_{20}$]-15-oxoETE stable isotope internal standard

(ISTD) were synthesized in-house as previously reported (11). Peroxide free arachidonic acid, 17-oxoDHA, 5-oxoETE-d_7, 15-ketoPGE$_2$, 13,14-dihydro-15-ketoPGE$_2$, and 13,14-dihydro-15-ketoPGE$_2$-d_4 were purchased from Cayman Chemical (Ann Arbor, MI). Ammonium formate, glacial acetic acid, β-mercaptoethanol and dimethyl sulfoxide (DMSO) were purchased from Sigma-Aldrich (St. Louis, MO). HPLC grade chloroform as well as Optima LC/MS grade methanol, acetonitrile, water, isopropanol, ammonium acetate, and formic acid were purchased from Fisher Scientific (Pittsburgh, PA). Ham's F-12K media, Medium 200, HBSS, low serum growth supplement (LSGS) kit, human umbilical vein endothelial cells (HUVECs), streptomycin, and penicillin were purchased from Invitrogen (Carlsbad, CA). Fetal bovine serum (FBS) was from Gemini Bioproducts (West Sacramento, CA). Human lung adenocarcinoma A549 cells (CRM-CCL-185) were obtained from ATCC (Manassas, VA).

Cell treatment with oxo-fatty acids. HUVECs were grown until 80% confluence on Collagen IV coated plates from Becton Dickinson (Bedford, MA), and maintained in medium 200 supplemented with LSGS. Cells were treated with 10 µM 11-oxoETE, 11-oxoETE-ME, 15-oxoETE, or 15-oxoETE-ME in 0.25% DMSO containing media. A549 cells were grown to 80% confluency Ham's F12K media containing 10% FBS and 1% pen/strep. All cells were maintained at 37 °C with 5% CO_2. At the time of treatment, media was replaced with HBSS and 10 µM 15-oxoETE or 17-oxoDHA in 0.25% DMSO was added to A549 cells. An initial treatment time of 90 minutes at 37˚C was chosen based on previously published uptake data (14, 23). In targeted experiments, either 2.5 ng of [$^{13}C_{20}$]-15-oxoETE or 20 ng of 5-oxoETE-d_7 as indicated was added as an internal standard (ISTD) and the extraction was performed as previously described with minor modifications (24). Briefly, cells were lifted with a scraper, mixed, and an aliquot of the resulting suspension was transferred to a glass tube. Folch extractions were performed with 2 volumes of 2:1 $CHCl_3$:MeOH with 0.1% acetic acid. The organic phase was evaporated to dryness under N_2. The samples were dissolved in 100 µL 70:30 H_2O:CH_3CN with 0.1% formic acid and filtered through Costar centrifuge filters (0.22 µm nylon) before transfer into HPLC vials for LC-HRMS analysis.

HUVEC Reduction Time Course. Media containing 0.25% DMSO with 10 µM 11-oxo-ETE, 11-oxoETE-ME, 15-oxoETE, or 15-oxoETE-ME was added to HUVECs and the cells were incubated at 37˚C for 5 min, 30 min, 90 min, 3 h, 6 h or 9 h. At each time point, 450 µL of the supernatant media was collected and transferred to a glass tube. The cells were gently scraped in the remaining 450 µL of media and transferred to a glass tube. 2.5 ng of [$^{13}C_{20}$]-15-oxoETE ISTD was added followed by subsequent Folch extraction as previously described (24). The organic phase was evaporated to dryness under N_2. The samples were dissolved in 100 µL of 70:30 H_2O:CH_3CN with 0.1% formic acid then filtered using 0.22 µm nylon centrifuge filters and transferred into HPLC vials for LC-high resolution mass spectrometry (LC-HRMS) analysis.

A549 Reduction Time Course. A549 WT cells, A549 Scramble, and A549 PTGR1 cells were treated with 10uM 15-oxoETE, 10uM 17-oxoDHA or 10uM 15-ketoPGE$_2$ (positive control) in 12 well plates when cells were at 80% confluency. The treatments lasted for 6 h with 5 collection time points (5 min, 30 min, 90 min, 3 h, and 6 h). Cell lysates were scraped in 1 mL of PBS and the internal standard, 5-oxoETE-d$_7$ (20 ng) was added before samples were extracted with 5 mL of $CHCl_3$:MeOH (2:1). Samples were vortexed and centrifuged at 2800 X g for 10 min. The organic layer was transferred to a new tube, dried under N_2 and stored at -80˚C before analysis.

PTGR1 shRNA knockdown. Lentiviral particles were generated by co-transfection of 4 plasmids [Control plasmid (pLKO.1-SCRshRNA-Puro) or one of the five different PTGR1-specific shRNA expressing plasmids, pLKO.1-shRNA-PTGR1.1-5 together with pMD2.g (VSVG), pVSV-REV and pMDLg/pRRE] into 293-FT cells using TransIT®-2020 Transfection reagent, with support from the UPCI Lentiviral Facility. The PTGR1-specific shRNAs target the following sequences in the PTGR1 gene: (1) CGTCTCCTGATGGTTATGATT, (2) GCCTACTTTGGCCTACTTGAA,(3) CTATCCTACTAATAGTGACTT, (4) CTTGGATTTGATGTCGTCTTT, and (5) GACTTGCTGAAATGGGTCTTA (Supplementary Table 1). The collection and isolation of lentiviral particles and A549 cell transduction were performed as described previously (9). Stable cell lines were

selected in puromycin (1 µg/ml) for 2 weeks. Knockdown (KD) of PTGR1 was confirmed by immunoblot and checked throughout experimentation. For PTGR1-KD cells, proteins were normalized to 15 µg/µL and each sample was loaded onto NuPAGE 4-12% Bis-Tris Midi Gel. Proteins on the gel were then transferred to nitrocellulose membrane and blocked in 5% non-fat dried milk in TBST for 1 h. The immunoblot was probed with 1:1000 PTGR1 rabbit antibody for 24 h (Aviva Systems Biology, San Diego, CA) and a horseradish peroxidase-conjugated anti-rabbit secondary antibody for 1 h. Membranes were visualized using BioRad Chemi-doc (Hercules, CA).

LC-MS discovery and validation of oxo-fatty acid metabolites. For LC-HRMS analysis, LC separations were conducted as previously described (22) using a Waters nano-ACQUITY UPLC system (Waters Corp., Milford, MA, USA). A Waters XBridge BEH130 C18 column (100 µm × 150 mm, 1.7 µm pore size; Waters Corp) was employed for reversed phase separation with a 3 µL injection. For gradient 1, used during discovery and targeted validation experiments, the flow-rate was 1.8 µL/min, solvent A was 98:2 water/acetonitrile (v/v) with 0.1% formic acid, and solvent B was 99.5:0.5 acetonitrile/water (v/v) with 0.1% formic acid. The gradient was as follows: 2% B at 0 min, 2% B at 3 min, 3.6% B at 11 min, 8% B at 15 min, 8% B at 27 min, 50% B at 30 min, 50% at 35 min, and 2% B at 37 min. Separations were performed at 30°C. For gradient 2, used for the confirmation of MS/HRMS and adduct studies with BME and GSH, the flow-rate was 1.5 µL/min, solvent A was 4:6 water/acetonitrile (v/v) with 0.1% formic acid and 10 mM ammonium formate and solvent B was 1:9 acetonitrile/isopropanol (v/v) with 0.1% formic acid and 10 mM ammonium formate. The gradient was as follows: 30% B at 0 min, 30% B at 6 min, 60% B at 11 min, 60% B at 15 min, 80% B at 27 min, 80% B at 30 min, 85 % at 35 min, 85 % at 45 min, 30 % at 47 min, and 30% B at 55 min. Separations were performed at 50°C. HRMS analysis was conducted using an LTQ XL-Orbitrap hybrid mass spectrometer (Thermo Fisher) in either positive or negative ion mode with a Michrom captive spray ESI source as previously described (22). For gradient 1 from above, the operating conditions were: spray voltage at 4 kV; capillary temperature at 250°C; capillary voltage at 35 V, tube lens 60 V. For gradient 2, the operating conditions were: spray voltage at

1.5 kV; capillary temperature at 200°C; capillary voltage at 0 V, tube lens 80 V. Analysis of differential abundant features was carried out by SIEVE 2.0, Metaboanalyst 2.0, and XCMS (26,27). Metabolic discovery experiments conducted in HUVEC cells revealed a diversity of differentially abundant features from the lipid fraction as demonstrated by the respective cloud plots generated with XCMS. A ranked list by fold change versus control using a *t*-test (Welch's unpaired) and a p-value cut-off of $p < 0.01$ was generated.

LC-MS/MS Characterization in A549 Cells. For the analysis of 15-oxoETE and 17-oxoDHA metabolism in A549 cells with and without PTGR1 shRNA KD and Scr shRNA control the samples were run in negative ion mode on a Sciex 6500 triple quadrupole ion trap coupled to a Shimadzu LC controller/pump and CTC Pal autosampler. A Phenomenex Luna C18(2) , 2 X 100 mm was used for separation with a gradient of H_2O + 0.1% acetic acid (A) and ACN + 0.1% acetic acid (B) using a flow rate of 0.6 mL/min. Solvent B started at 30% and increased to 100% B over 11 min. B was held at 100% for 3 min before returning to initial conditions to equilibrate the column for 2 min. The α, β-unsaturated ketones and metabolites were analyzed using the following source conditions: DP -65, EP -10, CE-25, and CXP -12. The MS source parameters were the following: CAD 11, curtain gas 30, gs1 80, gs2 85, ISV -4500 and source temp 600 ˚C. The following transitions were monitored: 15-oxoETE: 317.2→113.2, dihydro-15-oxoETE: 319.2→221.2, 15-HETE: 319.2→219.2, 5-oxoETE-d_7: 324.2→210.2, 17-oxoDHA: 341.2→297.2, 17-HDoHE: 343.2→273.2. dihydro-17oxoDHA: 343.2→299.2, 15-ketoPGE$_2$: 349.2→161.2, 13,14-dihydro-15-ketoPGE$_2$: 351.2→235.2, and 13,14-dihydro-15-ketoPGE$_2$-d_4: 355.2→239.2. Confirmation of the position of double bond saturation was performed on a Thermo Fisher Q Exactive coupled to a Vanquish UHPLC using the same gradient described above. Samples were analyzed using full scan and parallel reaction monitoring, at a resolution of 35K and fragment ions were confirmed using accurate mass < 5ppm.

Results

Untargeted discovery reveals distinctive patterns of oxoETEs metabolism in HUVECs. To determine possible routes of 11-oxoETE and 15-oxoETE metabolism, HUVECs were treated for 90 min with 10 μM of each compound. LC-HRMS was conducted in an untargeted manner on the extracted organic (lipid) and aqueous fractions. Analysis of differential abundant features was carried out and the top 25 features based on fold change and p-value from each analysis were manually curated and representative chromatograms were extracted from raw data samples (www.xcmsonline, Job #1198294 and 1198300). Two sequential mass shifts of +2 amu (proposed mono and di-saturated species) and an increased retention time were chosen for follow up targeted analysis for 11-oxoETE (Fig. 1A), as this pathway of metabolism has not been reported previously. Only one +2 amu shift (mono-saturated) was observed for 15-oxoETE (Fig. 1B). These putative 15-oxoETE metabolites were confirmed by comparison to the treatment of HUVECs with [$^{13}C_{20}$]-15oxoETE (Fig. 1C). This pattern of retention time and mass shift seems logically indicative of a reduction in double bonds. Accurate mass matched predicted values for both parent and saturated compounds for 11-oxoETE and 15-oxoETE in positive and negative ion mode within 2.5ppm, so a 5ppm window was selected to extract all ion chromatograms.

Time course studies reveal accumulation of saturated metabolites. HUVECs were treated as described above, using 11-oxoETE or 15-oxoETE over 9 hr. The area of the target peak was integrated and expressed as a ratio over the area of the [$^{13}C_{20}$]-15-oxoETE ISTD peak that was spiked into the samples immediately before extraction. Values were expressed as the ratio of analyte area/ISTD for each time point. For 11-oxoETE, both mono (Fig. 2A), and di-saturated (Fig. 2B) products appeared at the 5 min time point and accumulated over time in cell lysate (Fig. 2). Accumulation over time of the mono-saturated 15-oxoETE (Fig. 2C) metabolite was similarly observed. HUVECs were also treated with methyl ester derivatives of 11-oxoETE and 15-oxETE and showed the same metabolite formation, but at an order of magnitude greater accumulation of the metabolites compared to cells treated with the free acids, 11- and 15-oxoETE (data not shown). This was in agreement with our previous work

demonstrating that treatment of cells with the methyl esters of oxoETEs, increased the intracellular pool of the free oxoETEs (25).

MS/MS of parent oxoETEs and saturated metabolites. LC-MS/MS with CID fragmentation was utilized to elucidate the structure of the 11-oxoETE (Fig. 3A) and its corresponding metabolites. Under the described LC-MS conditions, 11-oxoETE (*m/z* 317.2122) eluted at 5.5 minutes and extracted MS^2 fragment ion species of *m/z* 299.2015, *m/z* 273.2222, and *m/z* 211.1341 also demonstrated corresponding peaks at this retention time (Fig. 3B). As predicted, mono-saturated 11-oxoETE (*m/z* 319.2273) (Fig. 3C) and di-saturated 11-oxoETE (*m/z* 321.2429) (Fig. 3D) species eluted at later retention times on the reversed phase column. Corresponding diagnostic MS^2 fragment ions were +2 (*m/z* 301.2172 and *m/z* 275.2380) and +4 amu (*m/z* 303.2328 and *m/z* 277.2535) higher than those for 11-oxoETE. The 11-oxoETE MS/MS spectrum exhibited *m/z* 165.1286 (δ = 0.6ppm) that is formed by α-cleavage to the carbonyl at C11 (Fig. 3B). The MS/MS spectrum of the mono-saturated 11-oxoETE retained the fragment at *m/z* 211.1341, but the *m/z* 165.1286 was absent, instead *m/z* 167.1443 was present, indicating that the first saturation took place at the C14-C15 double bond (Fig. 3C). The *m/z* 211.1341 was not present in the di-saturated metabolite and the *m/z* 167.1443 was still present (Fig. 3D) thus inferring that the electrophilic double bond was saturated. However, further experiments were needed to differentially determine a saturation at C12-C13 vs C14-C15 for the mono- and di-saturated metabolites, with critical implications of the electrophilic character of 11-oxoETE.

The negative ion MS/MS spectrum of 15-oxoETE (Fig. 4A) was identical with published CID spectrum by MacMillan, *et. al* (26) and diagnostic fragment ions at *m/z* 219.1755, *m/z* 203,1080, and *m/z* 113.0977 (Fig. 4B) at a retention time of 5.1 min. As would be expected from the published spectra, the MS/MS spectrum of the mono-saturated 15-oxoETE contained fragment ions with a mass increase of +2 amu compared to 15-oxoETE, including *m/z* 319.2268, *m/z* 221.1545, and *m/z* 205.1236 at a later retention time of 5.4 min (Fig. 4C). The best described fragmentation of 15-oxoETE is due to the breaking of the double bond allylic to the carbonyl moiety. This generates the fragments *m/z* 113.0977,

corresponding to the part of the molecule without any other double bonds, and *m/z* 219.1394, corresponding to the part of the molecule containing all of the remaining double bonds (Fig. 4A). The MS/MS spectrum of the mono-saturated 15-oxoETE did show an intense fragment at 113.0977 strongly suggesting that the first reduction did not occur at C13-C14. The fragment corresponding to the *m/z* 219.1394 shifted to *m/z* 221.1549 is consistent with the first reduction taking place at either the C5-C6, C8-C9 or C11-C12 double bond. However, we can postulate that saturation of 15-oxoETE to form the mono-saturated product likely occurs at the C5-C6 double bond as the fragment at *m/z* 165.1273, corresponding to the chemical composition $C_{11}H_{17}O$ found in 15-oxoETE is also accompanied by a fragment at *m/z* 167.1066 in the mono-saturated product (Fig. 4D). This fragment corresponds to the chemical composition $C_{10}H_{15}O_2$, a fragment adjacent to the C8-C9 double bond that would likely not be present if saturation occurred at this position.

Michael addition adducts reveal the position of double bond reduction. To further elucidate the points of saturation for 11- and 15-oxoETE, we examined the formation of GSH-adducts from treated HUVECs by LC-HRMS. GSH-adducts were observed for the parent and mono-saturated 11-oxoETE (Fig. 5A) and the parent and mono-saturated 15-oxoETE (Fig. 5B). No GSH-adduct was observed for the di-saturated 11-oxoETE metabolite, confirming C12-C13 double bond saturation and thus loss of the electrophilic α, β-unsaturated carbonyl (Fig. 5A). The two peaks for the parent 11-oxoETE-GSH adduct correspond to the 1,4- and the 1,6-Michael addition products. Supporting the identification of the initial saturation of 11-oxoETE at the C14-15 double bond, the mono-saturated product displayed only one peak, which would be the case if the 1,6-Michael product could no longer form due to C14-15 double bond saturation (14, 27).

Confirmation of 15-oxoETE metabolism in A549 cells. A549 cells were treated with 10 µM 15-oxoETE and samples were taken at time 0, 5 min, 30 min, 90 min, 3 and 6 h for targeted LC-MS/MS analysis. The metabolism of 15-oxoETE to a mono-saturated metabolite was demonstrated to be the similar in A549 cells as the HUVECs (Fig. 6A). Formation of the mono-saturated 15-oxoETE metabolite

occurred rapidly within the first 1.5 h and steadily climbed until 3 h where it plateaued . Cell lysates were analyzed using high resolution MS on a Thermo Q Exactive coupled to a Vanquish UHPLC using the same gradient as the initial analysis to further characterize the mono-saturated species using parallel reaction monitoring. The fragmentation seen in A549 cells corresponds to that seen in HUVECs with the primary saturation taking place at the non-electrophilic double bond (Fig. 6B and C)

The mono-saturated metabolite of the Ω-3 fatty acid 17-oxoDHA retains electrophilicity. A549 cells were exogenously administered 10 μM 17-oxoDHA, the oxo derivative of the Ω-3 fatty acid, docosahexaenoic acid. Treatment followed the same time course described above and formation of the mono-saturated metabolite peaked around 3 h in cell lysate (Fig. 6A). The mono-saturated product of 17-oxoDHA was characterized using LC-HRMS on the Q Exactive. The primary point of 17-oxoDHA saturation is more readily distinguished as the major fragment *m/z* 111.0801 (Fig. 7B) is shifted to 113.0957 (Fig. 7C). This *m/z* corresponds to fragmentation across the C7-C8 position indicating that saturation has occurred at the Ω-3 position and not at the α,β-unsaturated double. These results demonstrate that this metabolism is not unique to the arachidonic acid-derived oxoETEs metabolites or to HUVEC cells.

Prostaglandin reductase saturates non-electrophilic double bonds. There are numerous dehydrogenases and reductases that may be responsible for the saturation of fatty acid double bonds (28). Prostaglandin reductase, PTGR1, is best known for the saturation of the α,β-double bond of 15-ketoPGE$_2$, thus forming the non-electrophilic metabolite, 13,14-dihydro-15-ketoPGE$_2$. Due to the similarity in structure between PGE$_2$ and the oxoETEs it would seem plausible that PTGR1 would also reduce the α,β-unsaturated double bond of 15-oxoETE, 11-oxoETE and possibly even 17-oxoDHA. In order to demonstrate a possible role for PTGR1, we used lentiviral shRNA to knockdown PTGR1 protein expression via RNA interference (Table 1). A549 cells were transduced with lentivirus expressing control (Scr, scrambled shRNA) or PTGR1-specific shRNA. Western blot analysis indicates a ~50% knockdown (KD) of PTGR1 protein expression as compared to control and Scr (Fig. 8A). PTGR1-KD,

Scr, and control A549 cells were treated with 10 μM 15-oxoETE and metabolites were analyzed using targeted analysis on the Sciex 6500 QTrap. No differences in 15-oxoETE metabolism were observed between A549 WT and Scr after 15-oxoETE treatment. However, PTGR1-KD cells displayed a significant decrease in the ratio of the mono-saturated metabolite/15-oxoETE at 3 and 6 h (Fig. 8B). Similarly, a significant decrease in the ratio of mono-saturated/17-oxoDHAwas observed at 3and 6 h (Fig. 8C). 15-ketoPGE$_2$ was used as the positive control and a significant decrease in 13,14-dihydro-15-ketoPGE$_2$ was observed starting at 30 min and continued throughout the rest of the experiment (Fig. 8D). While PTGR1 does appear to play a role in 15-oxoETE and 17-oxoDHA metabolism, the decrease in the formation of the mono-saturated species in the PTGR1-KD cells is not as significant as 15-ketoPGE$_2$ suggesting that other reductases are also capable of saturating double bond positions alternative to the electrophilic α, β double bond.

Discussion

The study of fatty acid metabolism has mostly focused on the formation of first generation bioactive lipids (i.e. HETEs, leukotrienes, PGs) and their signaling abilities, while downstream metabolism of these species remains poorly characterized. Existing literature on eicosanoid metabolism for COX/15PGDH products has focused on PGE$_2$ and its 15PGDH dependent electrophilic product 15-ketoPGE$_2$, previously thought to be inactive; however, numerous studies including those focused on nitro-fatty acids have overwhelmingly demonstrated that electrophilic fatty acids are conferred with redox signaling capabilities (6, 8, 19, 29, 30). Further metabolism of 15-ketoPGE$_2$ occurs via double bond reduction by PTGR1 to form the non-electrophilic product 13,14-dihydro-15-keto-PGE$_2$. The electrophilic fatty acids 11- and 15-oxoETE are also products of 15PGDH and it would seem logical that reduction to a non-electrophilic metabolite would follow the same pathway as 15-ketoPGE$_2$. However, this was not the case for either of these AA-derived bioactive lipids 11-oxoETE and 15-oxoETE, nor the DHA-derived electrophile, 17-oxoDHA (Scheme 1). In this work, we expand the knowledge of these pathways to include additional downstream products.

Our untargeted metabolomics approach revealed a distinct pattern of limited saturation for 11- and 15-oxoETE. The similar metabolism of [$^{13}C_{20}$]-15oxoETE, as well as time course studies support that these metabolites are derivatives of the parent oxoETEs. By examining the formation of GSH-derived Michael adducts we were able to discern the electrophilic status of the double bond proximal to the carbonyl in the α,β-unsaturated ketone moiety of the oxoETEs. The parent and predominant first saturation product of 11- and 15-oxoETE maintain electrophilicity, hence the α,β-unsaturated ketone moiety. However, the second saturation of 11-oxoETE no longer forms a GSH adduct, indicating the double bond at C12-C13 adjacent to the carbonyl has been reduced. The enzymatic basis of this transformation warrants investigation as the α,β-unsaturated ketone moiety has been associated with bioactivity in related molecules. These results were recapitulated in A549 cells and were also found to be relevant to the metabolism of the Ω-3 metabolite, 17-oxoDHA, which is also a bioactive lipid capable of activating the Nrf2 antioxidant response and inhibiting NF-κB-derived pro-inflammatory signaling (16).

To determine if PTGR1 plays a role in the metabolism of oxoETEs and oxoDHA species, we transduced A549 cells with lentivirus expressing control or PTGR1-specific shRNA and monitored the formation of saturated metabolites in cell lysate. Western blot demonstrated a 50% knockdown of PTGR1 protein expression in A549 cells and 15-ketoPGE$_2$ was used as a positive control in the cell metabolism studies. PTGR1 KD significantly decreased formation of the mono-saturated metabolite when 15-oxoETE and 17-oxoDHA substrates were used, although not until 3 hr, whereas saturation of the positive control, 15-ketoPGE$_2$ was significant as early at 30 min (Fig. 8). At the later time points, inhibition of saturation in PTGR1-KD cells was similar. 15-ketoPGE$_2$ conversion to 13,14-dihydro-15-oxoPGE$_2$ was decreased by ~4.4-fold at 3 hr, whereas formation of the mono-saturated metabolite decreased ~2-fold and ~4.9-fold for 15-oxoETE and 17-oxoDHA, respectively. This implies that other reductases have similar preferences for the double bond reduction of these fatty acid metabolites and may compensate for the loss of PTGR1 (Scheme 1).

Critical examination of oxo-fatty acid metabolism is warranted in light of the acceptance of electrophiles as FDA-approved therapeutics (dimethyl-fumarate)(31) and the extensive number of studies published on electrophilic oxo- and nitro-fatty acid signaling (8, 10, 32). Thus, we sought out to characterize the primary metabolic products of oxo-fatty acids in order to better understand their normal and pathological functions. Metabolic pathway characterization will also help to facilitate identification of the enzyme(s) responsible for the saturation of the electrophilic double bond. A variety of distinct fatty acid metabolizing enzymes exist with varying specificity for substrate and reaction (7) and there are numerous short and medium chain dehydrogenases/reductases that are still classified as orphans. Elucidation of the pathways of metabolism will also allow for the design of therapeutic interventions to modulate or mimic the effects of these molecules, and aid in the discovery of inhibitors or the design of stable derivatives. As an additional benefit, identification of these novel metabolites may contribute to the ongoing efforts in untargeted metabolomics to build high resolution databases as well as an increased appreciation of specificity in lipidomics experiments.

Acknowledgements. This work was supported by the National Institutes of Health P30ES013508 (IAB), K22ES26235 and R21HD087866 (NWS), UL1TR000005 and R21AI12207 (Wendell), R01CA148629 (Sobol) and the Abraham A. Mitchell Distinguished Investigator fund to RWS. Support for the UPCI Lentiviral Facility was provided by the Cancer Center Support Grant from the National Institutes of Health [CA047904]. SGW declares interest in Complexa Inc. RWS is a scientific consultant for Trevigen, Inc.

References

1. Smyth, E. M., T. Grosser, M. Wang, Y. Yu, and G. A. FitzGerald. 2009. Prostanoids in health and disease. *Journal of lipid research* **50 Suppl**: S423-428.
2. Funk, C. D. 2001. Prostaglandins and leukotrienes: advances in eicosanoid biology. *Science* **294**: 1871-1875.
3. Jamieson, K. L., T. Endo, A. M. Darwesh, V. Samokhvalov, and J. M. Seubert. 2017. Cytochrome P450-derived eicosanoids and heart function. *Pharmacology & therapeutics*.
4. Arnold, C., M. Markovic, K. Blossey, G. Wallukat, R. Fischer, R. Dechend, A. Konkel, C. von Schacky, F. C. Luft, D. N. Muller, M. Rothe, and W. H. Schunck. Arachidonic acid-metabolizing cytochrome P450 enzymes are targets of {omega}-3 fatty acids. *J Biol Chem* **285**: 32720-32733.
5. Needleman, P., J. Turk, B. A. Jakschik, A. R. Morrison, and J. B. Lefkowith. 1986. Arachidonic acid metabolism. *Annual review of biochemistry* **55**: 69-102.
6. Delmastro-Greenwood, M., B. A. Freeman, and S. G. Wendell. 2014. Redox-dependent anti-inflammatory signaling actions of unsaturated fatty acids. *Annual review of physiology* **76**: 79-105.
7. Tai, H. H., C. M. Ensor, M. Tong, H. Zhou, and F. Yan. 2002. Prostaglandin catabolizing enzymes. *Prostaglandins & other lipid mediators* **68-69**: 483-493.
8. Snyder, N. W., F. Golin-Bisello, Y. Gao, I. A. Blair, B. A. Freeman, and S. G. Wendell. 2014. 15-Oxoeicosatetraenoic acid is a 15-hydroxyprostaglandin dehydrogenase-derived electrophilic mediator of inflammatory signaling pathways. *Chemico-biological interactions*.
9. Wendell, S. G., F. Golin-Bisello, S. Wenzel, R. W. Sobol, F. Holguin, and B. A. Freeman. 2015. 15-Hydroxyprostaglandin dehydrogenase generation of electrophilic lipid signaling mediators from hydroxy omega-3 fatty acids. *J Biol Chem* **290**: 5868-5880.
10. Schopfer, F., C Cipollina and BA Freeman. 2011. Formation and signaling actions of electrophilic lipids. *Chem Rev* **111**: 5997-6021.
11. Shiraki, T., N. Kamiya, S. Shiki, T. S. Kodama, A. Kakizuka, and H. Jingami. 2005. Alpha,beta-unsaturated ketone is a core moiety of natural ligands for covalent binding to peroxisome proliferator-activated receptor gamma. *J.Biol.Chem.* **280**: 14145-14153.
12. Grant, G. E., J. Rokach, and W. S. Powell. 2009. 5-Oxo-ETE and the OXE receptor. *Prostaglandins & other lipid mediators* **89**: 98-104.
13. Baker, P. R., F. J. Schopfer, V. B. O'Donnell, and B. A. Freeman. 2009. Convergence of nitric oxide and lipid signaling: anti-inflammatory nitro-fatty acids. *Free Radic Biol Med* **46**: 989-1003.

14. Liu, X., S. Zhang, J. S. Arora, N. W. Snyder, S. J. Shah, and I. A. Blair. 2011. 11-Oxoeicosatetraenoic acid is a cyclooxygenase-2/15-hydroxyprostaglandin dehydrogenase-derived antiproliferative eicosanoid. *Chem Res Toxicol* **24**: 2227-2236.
15. Wei, C., P. Zhu, S. J. Shah, and I. A. Blair. 2009. 15-oxo-Eicosatetraenoic acid, a metabolite of macrophage 15-hydroxyprostaglandin dehydrogenase that inhibits endothelial cell proliferation. *Mol Pharmacol* **76**: 516-525.
16. Groeger, A. L., C. Cipollina, M. P. Cole, S. R. Woodcock, G. Bonacci, T. K. Rudolph, V. Rudolph, B. A. Freeman, and F. J. Schopfer. 2010. Cyclooxygenase-2 generates anti-inflammatory mediators from omega-3 fatty acids. *Nat Chem Biol* **6**: 433-441.
17. Bell-Parikh, L. C., T. Ide, J. A. Lawson, P. McNamara, M. Reilly, and G. A. FitzGerald. 2003. Biosynthesis of 15-deoxy-delta12,14-PGJ2 and the ligation of PPARgamma. *J Clin Invest* **112**: 945-955.
18. Scher, J. U., and M. H. Pillinger. 2005. 15d-PGJ2: the anti-inflammatory prostaglandin? *Clinical immunology* **114**: 100-109.
19. Chou, W. L., L. M. Chuang, C. C. Chou, A. H. Wang, J. A. Lawson, G. A. FitzGerald, and Z. F. Chang. 2007. Identification of a novel prostaglandin reductase reveals the involvement of prostaglandin E2 catabolism in regulation of peroxisome proliferator-activated receptor gamma activation. *J Biol Chem* **282**: 18162-18172.
20. Clish, C. B., B. D. Levy, N. Chiang, H. H. Tai, and C. N. Serhan. 2000. Oxidoreductases in lipoxin A4 metabolic inactivation: a novel role for 15-onoprostaglandin 13-reductase/leukotriene B4 12-hydroxydehydrogenase in inflammation. *J Biol Chem* **275**: 25372-25380.
21. Dick, R. A., M. K. Kwak, T. R. Sutter, and T. W. Kensler. 2001. Antioxidative function and substrate specificity of NAD(P)H-dependent alkenal/one oxidoreductase. A new role for leukotriene B4 12-hydroxydehydrogenase/15-oxoprostaglandin 13-reductase. *J Biol Chem* **276**: 40803-40810.
22. Vitturi, D. A., C. S. Chen, S. R. Woodcock, S. R. Salvatore, G. Bonacci, J. R. Koenitzer, N. A. Stewart, N. Wakabayashi, T. W. Kensler, B. A. Freeman, and F. J. Schopfer. 2013. Modulation of nitro-fatty acid signaling: prostaglandin reductase-1 is a nitroalkene reductase. *J Biol Chem* **288**: 25626-25637.
23. Snyder, N. W., S. D. Revello, X. Liu, S. Zhang, and I. A. Blair. 2013. Cellular uptake and antiproliferative effects of 11-oxo-eicosatetraenoic acid. *Journal of lipid research* **54**: 3070-3077.
24. Snyder, N. W., M. Khezam, C. A. Mesaros, A. Worth, and I. A. Blair. 2013. Untargeted metabolomics from biological sources using ultraperformance liquid chromatography-high resolution mass spectrometry (UPLC-HRMS). *Journal of visualized experiments : JoVE*: e50433.
25. Snyder, N. W., S. D. Revello, X. Liu, S. Zhang, and I. A. Blair. 2013. Cellular uptake and anti-proliferative effects of 11-oxo-eicosatetraenoic acid. *Journal of lipid research*.
26. MacMillan, D. K., and R. C. Murphy. 1995. Analysis of lipid hydroperoxides and long-chain conjugated keto acids by negative ion electrospray mass spectrometry. *J Am Soc Mass Spectrom* **6**: 1190-1201.
27. Lee, S. H., K. Rangiah, M. V. Williams, A. Y. Wehr, R. N. DuBois, and I. A. Blair. 2007. Cyclooxygenase-2-mediated metabolism of arachidonic acid to 15-oxo-eicosatetraenoic acid by rat intestinal epithelial cells. *Chem Res Toxicol* **20**: 1665-1675.
28. Bray, J. E., B. D. Marsden, and U. Oppermann. 2009. The human short-chain dehydrogenase/reductase (SDR) superfamily: a bioinformatics summary. *Chemico-biological interactions* **178**: 99-109.
29. Cipollina, C., S. R. Salvatore, M. F. Muldoon, B. A. Freeman, and F. J. Schopfer. 2014. Generation and dietary modulation of anti-inflammatory electrophilic omega-3 fatty acid derivatives. *PLoS One* **9**: e94836.
30. Bonacci, G., P. R. Baker, S. R. Salvatore, D. Shores, N. K. Khoo, J. R. Koenitzer, D. A. Vitturi, S. R. Woodcock, F. Golin-Bisello, M. P. Cole, S. Watkins, C. St Croix, C. I. Batthyany, B. A. Freeman, and F. J.

Schopfer. 2012. Conjugated linoleic acid is a preferential substrate for fatty acid nitration. *J Biol Chem* **287**: 44071-44082.
31. Bomprezzi, R. 2015. Dimethyl fumarate in the treatment of relapsing-remitting multiple sclerosis: an overview. *Ther Adv Neurol Disord* **8**: 20-30.
32. Woodcock, C. C., Y. Huang, S. R. Woodcock, S. R. Salvatore, B. Singh, F. Golin-Bisello, N. E. Davidson, C. A. Neumann, B. A. Freeman, and S. G. Wendell. 2018. Nitro-fatty acid inhibition of triple-negative breast cancer cell viability, migration, invasion, and tumor growth. *J Biol Chem* **293**: 1120-1137.

Table 1: PTGRI shRNA sequences

LCF Vector #	**Gene Name**	**Species**	**NM Id**	**Clone Name**	**Gene Symbol**	**Target Sequence** (the first 21 bases after CCGG of the Oligo Sequence)	**Oligo Sequence**
sh467.1	leukotriene B4 12-hydroxydehydrogenase	human	NM_012212	NM_012212.2-720s1c1	PTGR1	CGTCTCCTGATGGTTATGATT	CCGGCGTCTCCTGATGGTTATGATTCTCGAGAATCATAACCATCAGGAGACGTTTTT
sh467.2	leukotriene B4 12-hydroxydehydrogenase	human	NM_012212	NM_012212.2-488s1c1	PTGR1	GCCTACTTTGGCCTACTTGAA	CCGGGCCTACTTTGGCCTACTTGAACTCGAGTTCAAGTAGGCCAAAGTAGGCTTTTT
sh467.3	leukotriene B4 12-hydroxydehydrogenase	human	NM_012212	NM_012212.2-148s1c1	PTGR1	CTATCCTACTAATAGTGACTT	CCGGCTATCCTACTAATAGTGACTTCTCGAGAAGTCACTATTAGTAGGATAGTTTTT

sh467.4	leukotriene B4 12-hydroxydehydrogenase	human	NM_012212	NM_012212.2-656s1c1	PTGR1	CTTGGATTTGATGTCGTCTTT	CCGGCTTGGATTTGATGTCGTCTTTCTCGAGAAAGACGACATCAAATCCAAGTTTTT
sh467.5	leukotriene B4 12-hydroxydehydrogenase	human	NM_012212	NM_012212.2-959s1c1	PTGR1	GACTTGCTGAAATGGGTCTTA	CCGGGACTTGCTGAAATGGGTCTTACTCGAGTAAGACCCATTTCAGCAAGTCTTTTT

Figure 1

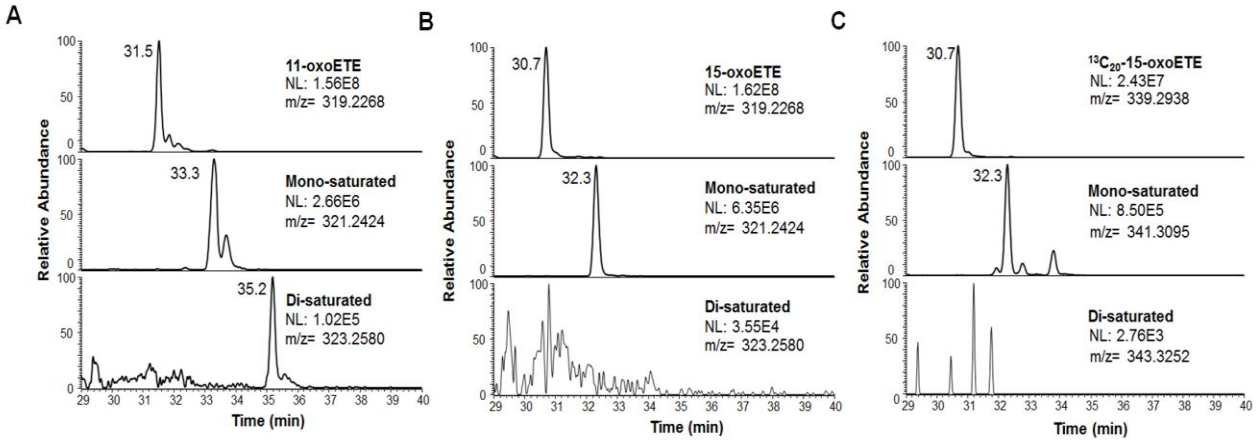

Figure 1: **Extracted ion chromatograms of LC-HRMS analysis of lipid extract from oxoETE treated HUVECs.** Mass spectral features from the discovery experiment were extracted from representative chromatograms with a 5 ppm mass window from the given *m/z* from positive ion mode LC-HRMS analysis of lipid extracts of HUVECs treated with (A) 11-oxoETE, (B) 15-oxoETE, (C)

[$^{13}C_{20}$]-15-oxoETE. Peaks putatively corresponding to double bond saturation were apparent for one and two saturations in 11-oxoETE. Only one saturation was detectable for 15-oxoETE and [$^{13}C_{20}$]-15-oxoETE.

Figure 2

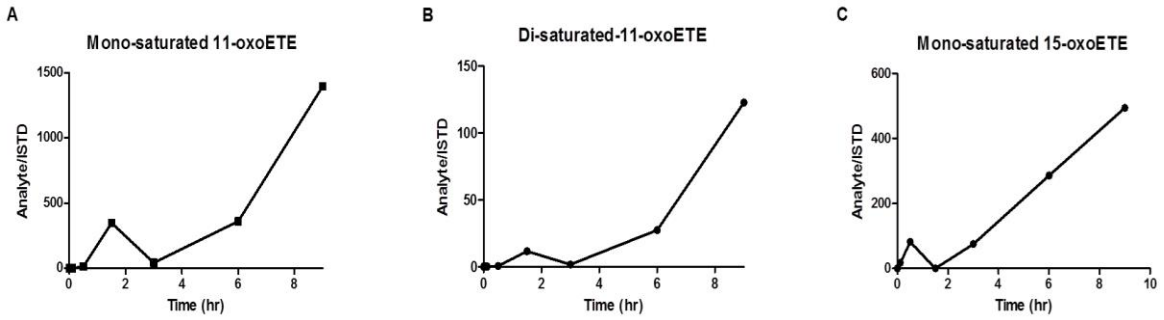

Figure 2: **Time course of oxoETE metabolite accumulation in HUVECs**. Accumulation of putative metabolites after treatment with 10 µM 11-oxoETE or 15-oxoETE. Area under the curve was calculated from XICs of metabolites. [$^{13}C_{20}$]-15-oxoETE was used as the internal standard and to normalize for extraction and ionization efficiency for relative quantitation. Values are expressed in area under the peak for (Analyte/ISTD) for the (A) mono-saturated 11-oxoETE metabolite, the (B) di-saturated 11-oxoETE metabolite and the (C) mono-saturated 15-oxoETE metabolite.

Figure 3

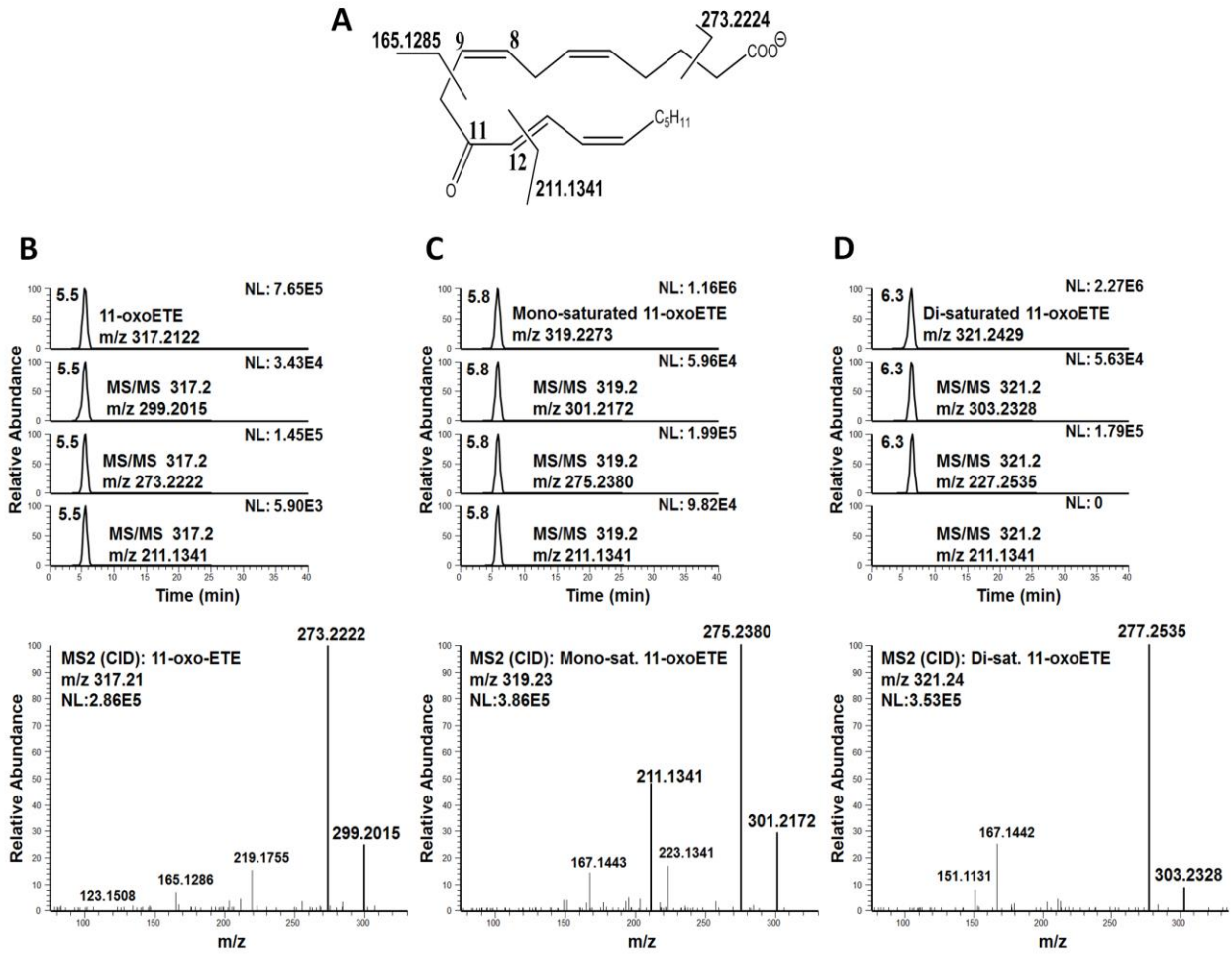

Figure 3: **LC-MS/HRMS confirmation of 11-oxoETE saturation products.** (A) 11-oxoETE structure and diagnostic fragmentation. Extracted chromatograms and product ion spectrum in negative ion mode for (B) 11-oxoETE (C) the mono-saturated 11-oxoETE metabolite, and (D) the di-saturated 11-oxoETE metabolite.

Figure 4

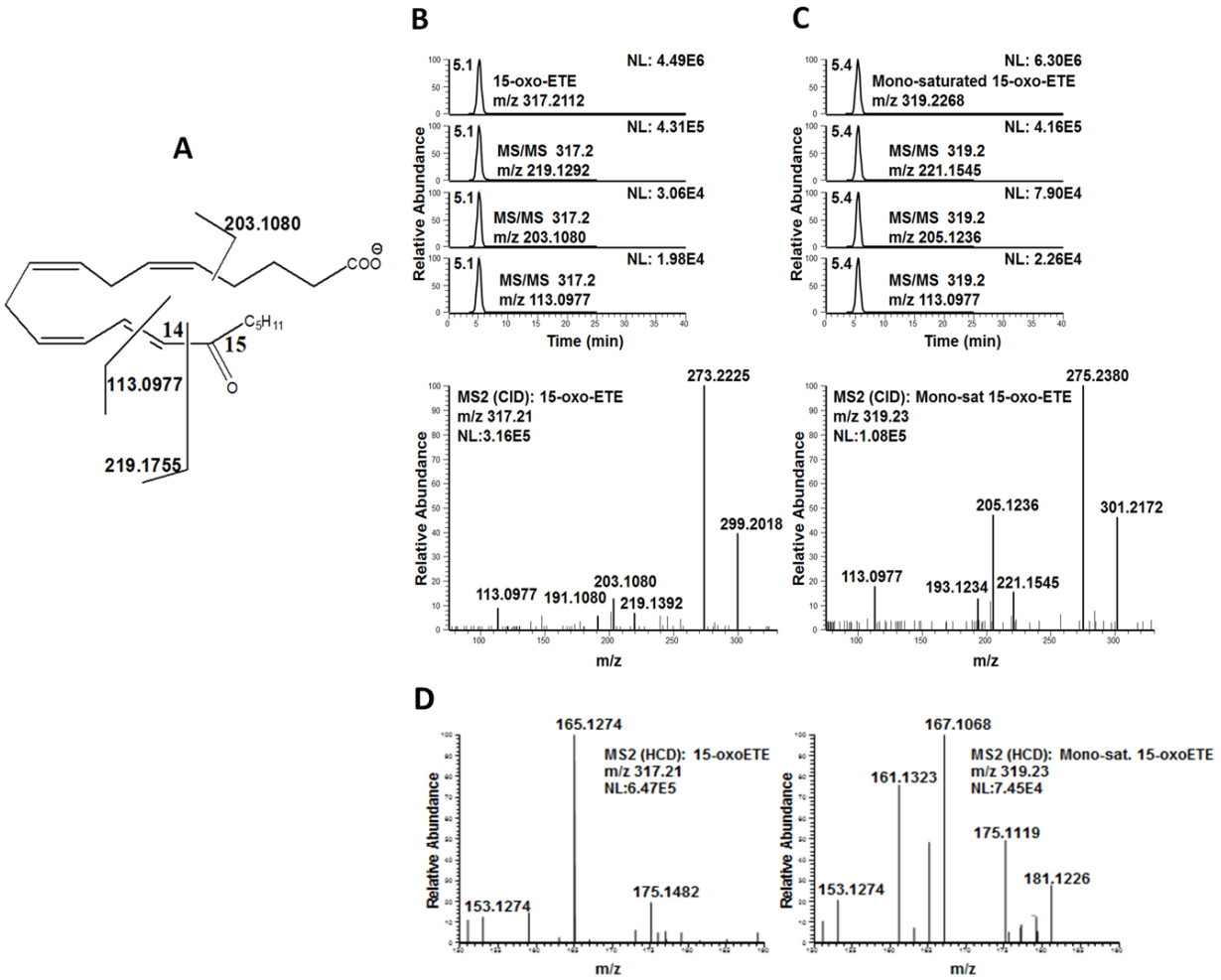

Figure 4: **LC-MS/HRMS confirmation of the 15-oxoETE saturation product.** (A) 15-oxoETE structure and diagnostic fragmentation. Extracted chromatograms and product ion spectrum in negative ion mode for (B) 15-oxoETE and (C) the mono-saturated 15-oxoETE metabolite. (D) Production ion spectra of 15-oxoETE and the mono-saturated 15-oxoETE metabolite between *m/z* 150-190 to highlight the fragmentation found at *m/z* 165.1274 for 15-oxoETE and *m/z* 167.1068 for the mono-saturated 15-oxoETE metabolite. The m/z of 167.1068 corresponds to fragmentation the chemical composition $C_{10}H_{15}O_2$, a fragment adjacent to the C8-C9 double bond that would likely not be present if saturation occurred at this position.

Figure 5

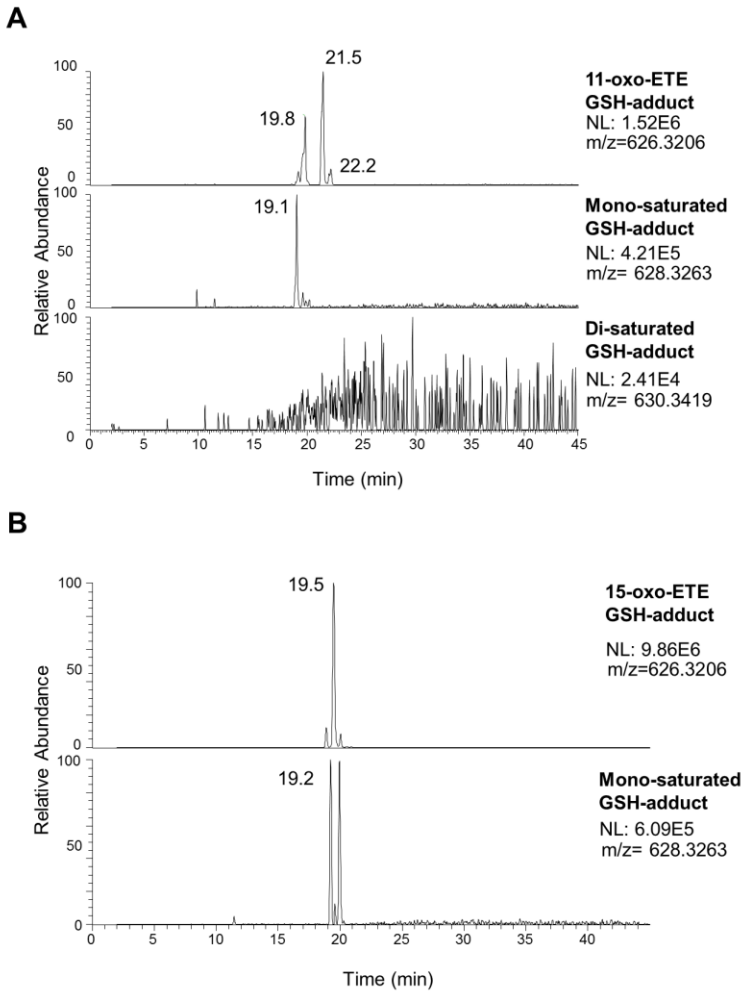

Figure 5: **LC-HRMS chromatograms of GSH-adducts from parent and saturated products of 11-oxo and 15-oxoETEs.** (A) 11-oxoETE, mono-saturated and di-saturated GSH conjugates (B) 15-oxoETE and its mono-saturated product.

Figure 6

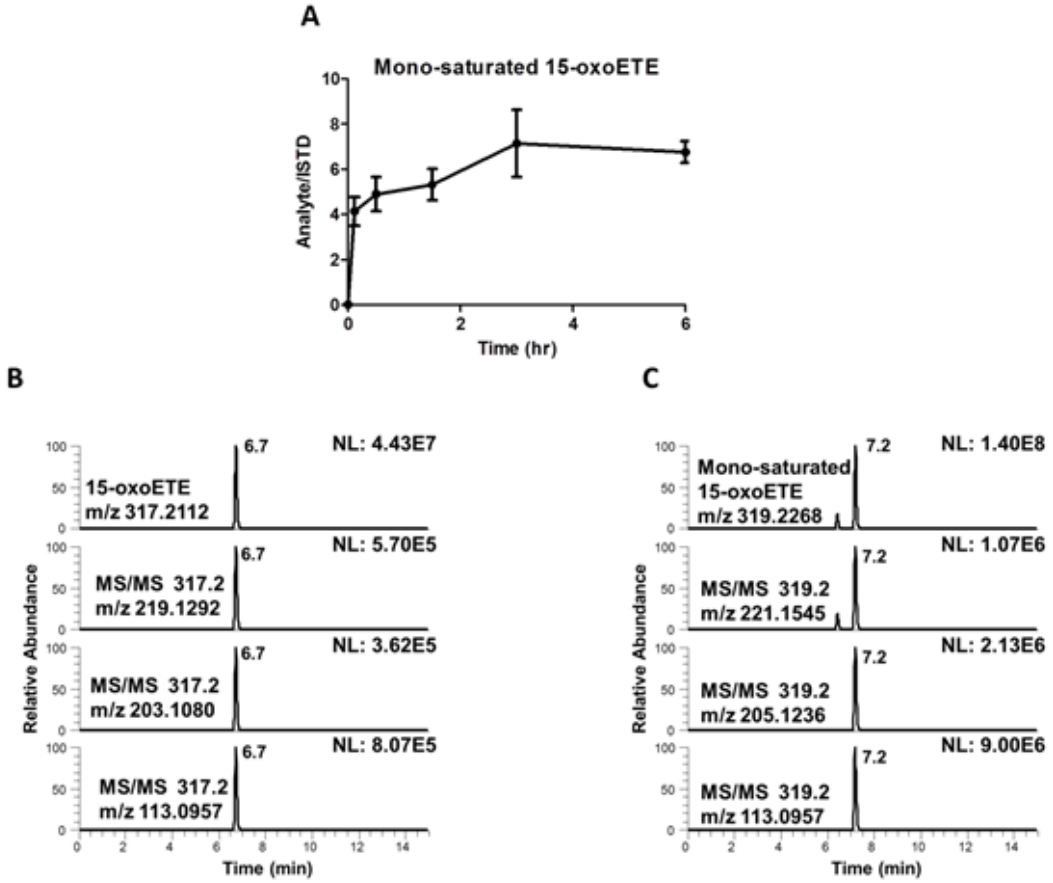

Figure 6: **15-oxoETE metabolism in A549 Cells**. (A) 15-oxoETE metabolism to the mono-saturated metabolite from 0 to 6 h. Extracted chromatograms of diagnostic product ions for (B) 15-oxoETE and (C) the mono-saturated 15-oxoETE metabolite.

Figure 7

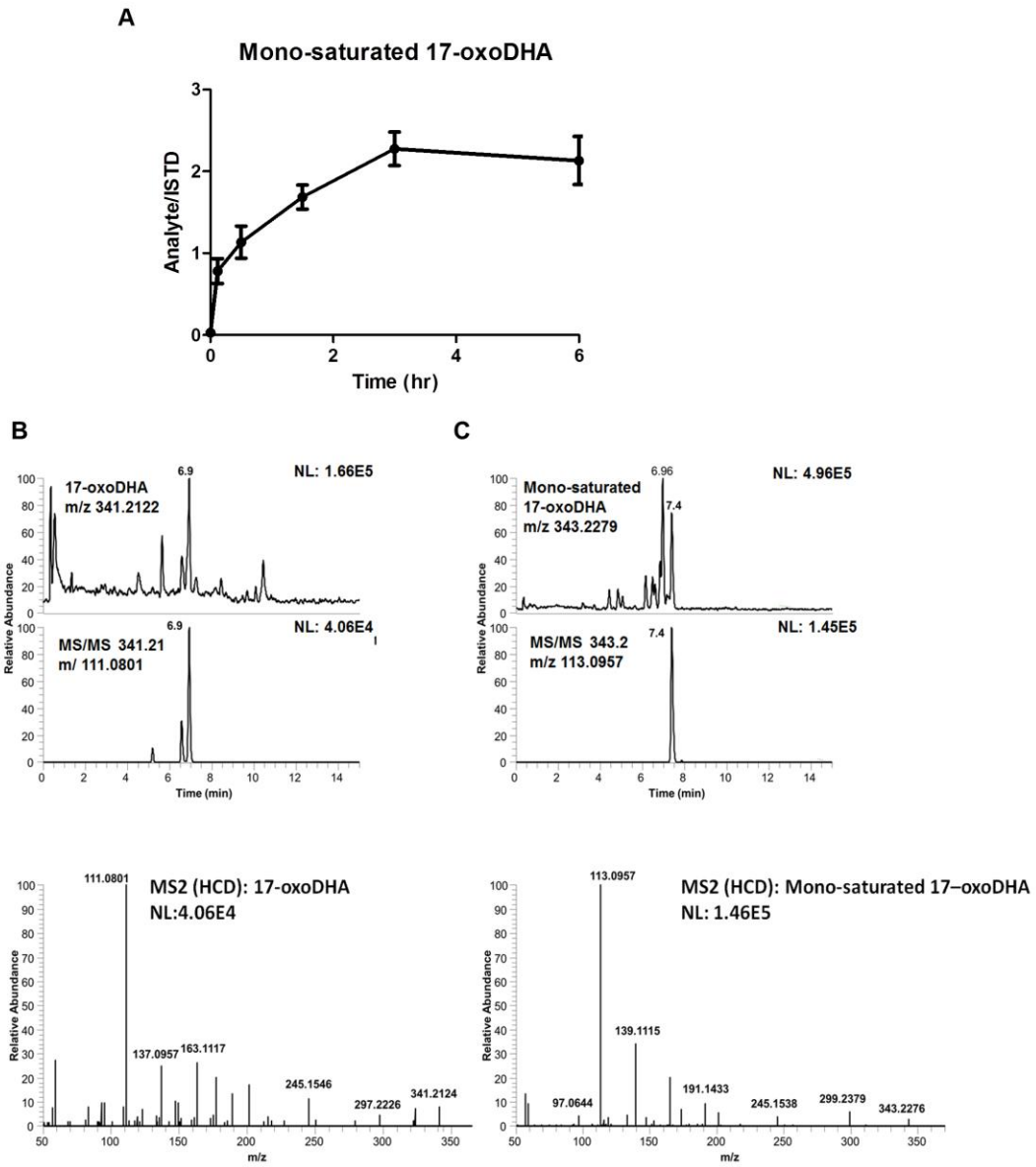

Figure 7: **17-oxoDHA metabolism in A549 Cells**. (A) 17-oxoDHA metabolism to the mono-saturated metabolite from 0 to 6 h. Extracted chromatograms of diagnostic product ions and product ion spectra for (B) 17-oxoDHA and (C) the mono-saturated 17-oxoDHA metabolite.

Figure 8

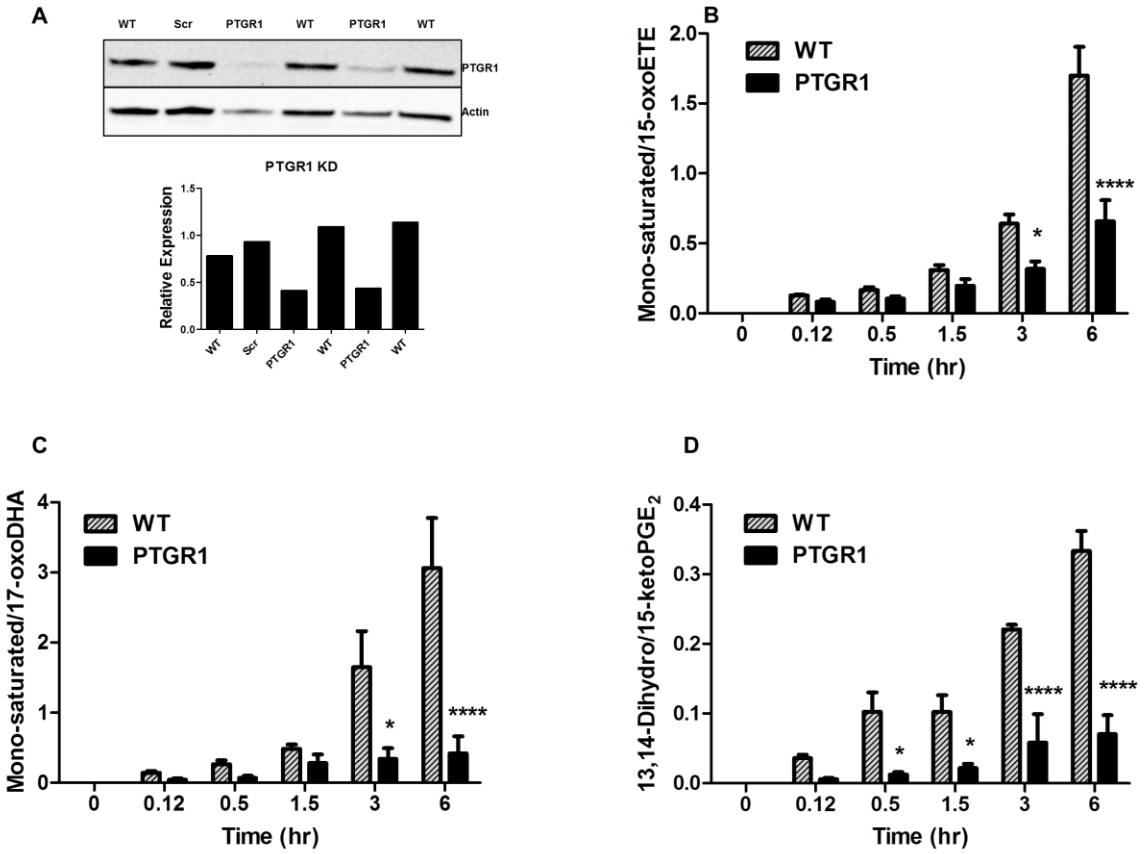

Figure 8: **PTGR1 KD in A549 cells partially abolishes electrophile metabolism**. (A) PTGR1 protein expression via western blot and image quantification Mono-saturated metabolite product/substrate ratio in A549 cell lysate for (B) 15-oxoETE, (C) 17-oxoDHA and the positive control (C) 15-ketoPGE$_2$.

Scheme 1

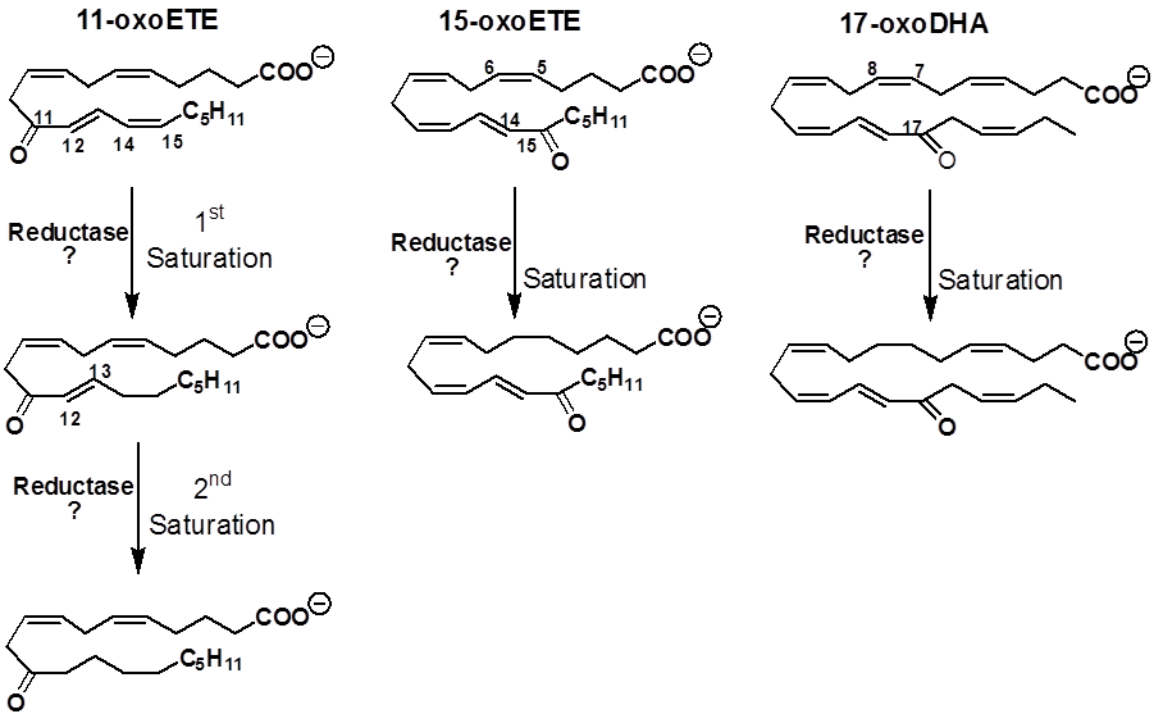

Scheme 1: Structures of 11-oxoETE, 15-oxoETE 17-oxoDHA and proposed saturation products. 11-oxoETE undergoes two rounds of saturation to form mono- and di-saturated metabolites whereas only mono-saturated metabolites were found for 15-oxoETE and 17-oxoDHA. Proposed points of saturation based off of the MS^2 spectra are also shown.